



ELSEVIER

Journal of Alloys and Compounds 293–295 (1999) 437–442

Journal of
ALLOYS
AND COMPOUNDS

Hydriding properties of the MgNi-based systems

S. Orimo^{a,*}, A. Züttel^b, K. Ikeda^{c,1}, S. Saruki^d, T. Fukunaga^e, H. Fujii^c, L. Schlapbach^b^aMax-Planck-Institut für Metallforschung, Heisenbergstrasse 1, 70569 Stuttgart, Germany^bUniversity of Fribourg, Physics Institute, Perolles 1700, Switzerland^cFaculty of Integrated Arts and Sciences, Hiroshima University, Higashi-Hiroshima 739-8521, Japan^dFaculty of Engineering, Nagoya University, Nagoya 464-01, Japan^eResearch Reactor Institute, Kyoto University, Osaka 590-0494, Japan

Abstract

In MgNi with an amorphous phase, a miscibility-gap (plateau) pressure of about 3×10^{-4} MPa at room temperature was clearly detected by electrochemical p - c isotherm measurements. The total radial distribution functions for X-ray and neutron diffraction indicated that deuterium in MgNi occupies an interstitial tetrahedral site composed of nearly 2Mg2Ni. Structural and hydriding properties of elemental substitution systems, Mg(Ni_{1-x}T_x) (T=Co and Cu) and (Mg_{1-x}Al_x)Ni with $x=0$ –0.5, were also investigated experimentally. © 1999 Elsevier Science S.A. All rights reserved.

Keywords: Magnesium–nickel; Hydrogen; Amorphous; Miscibility-gap; Substitution

1. Introduction

There are two intermetallic compounds in the Mg–Ni binary system, that is, Mg₂Ni and MgNi₂ [1]. Upon hydrogenation, Mg₂Ni transforms into the hydride phase Mg₂NiH₄, so as to form a stable covalent-type bonding composed of Mg²⁺ and [NiH₄]₄-complex [2–5]. On the other hand, MgNi₂ does not react with hydrogen at least in the crystalline phase [6].

In the equiatomic composition between the two compounds mentioned above, the amorphous MgNi phase is formed by mechanical alloying [7–14]. The maximum hydrogen content in MgNi corresponds to a composition of MgNiH_{1.9}; the pressure dependence of the hydrogen content is small compared with that in other amorphous alloys [11–13]. This hydrogen-to-metal ratio is valid for non-covalent-type hydrides such as TiFeH₂ with a CsCl(B2)-type structure. Therefore it is of importance to obtain accurate information on thermal stabilities and site-occupations of hydrogen in the MgNi-based systems.

The aims of this work were, first, to clarify the thermal stability and the site-occupation of hydrogen in MgNi itself [15], and then, to clarify the elemental substitution effects on MgNi [15–18].

2. Experimental procedure

The mixtures of Mg₂Ni (nearly 300 μm powder size), Co, Ni, Cu and Al (under 5 μm powder size) were mechanically alloyed under an argon atmosphere with a 5N5-purity, using a planetary ball mill apparatus (Fritsch P7) with 400 r.p.m. for 80 h at room temperature. The compositional ratios were $x=0$, 0.2 and 0.5 for Mg(Ni_{1-x}T_x) (T=Co and Cu), and $x=0$, 0.1, 0.2, 0.3, 0.4 and 0.5 for (Mg_{1-x}Al_x)Ni. For the neutron diffraction measurements at KEK, Tsukuba, Japan [19–21], the sample with $x=0$, MgNi, was deuterided under a deuterium atmosphere with a 4N-purity, using a Sieverts type apparatus under a 1.0 MPa at room temperature.

It should be emphasized that we paid particular attention to avoid impurity effects on the structural and hydriding properties of the samples [22]. The material and shape of the vial for mechanical alloying were carefully selected, so as to lower the amount of the elemental Fe contamination during mechanical alloying. In addition, the vial (equipped with a connection valve for evacuation or introduction of

*Corresponding author. Permanent address: Faculty of Integrated Arts and Sciences, Hiroshima University, Higashi-Hiroshima 739-8521, Japan. Fax: +81-824-24-0757.

E-mail address: orimo@ipc.hiroshima-u.ac.jp (S. Orimo)

¹Present address: Matsushita Battery Industrial Co., Ltd., Osaka 570-8511, Japan.

argon) with each sample was evacuated for 12 h below 0.01 Pa prior to mechanical alloying, and was always handled in a glove-box (filled with a purified argon of less than 0.5 p.p.m. oxygen, and of dew point with lower than 185 K), so as to minimize any oxidation or nitrogeation.

The structural and hydriding properties of the sample thus prepared were characterized by X-ray (Cu-K α radiation) and neutron diffraction measurements, high-resolution TEM observation, differential thermal analysis, and electrochemical p - c isotherm measurement. In the isotherm measurements [23–25], the discharge processes were measured with an equilibrium current of 20 mA g $^{-1}$, at room temperature.

3. Results and discussion

3.1. MgNi [11–15]

The process of mechanical alloying was examined by X-ray diffraction, which is shown in Fig. 1. The nanostructured Mg $_2$ Ni with broad diffraction peaks are already formed after 1 h, and then, the elemental Ni reacts with the nanostructured Mg $_2$ Ni to form the amorphous MgNi. The diffraction peaks corresponding to the elemental Ni are completely absent after 80 h. As shown in Fig. 2, neither Mg $_2$ Ni nor Ni crystallite can be microscopically observed after 80 h. In Ref. [26], the formation process of the amorphous phase was investigated by transmission electron microscopy.

The electrochemical p - c isotherm of MgNi is shown in Fig. 3.

We would like to emphasize that there is obviously a

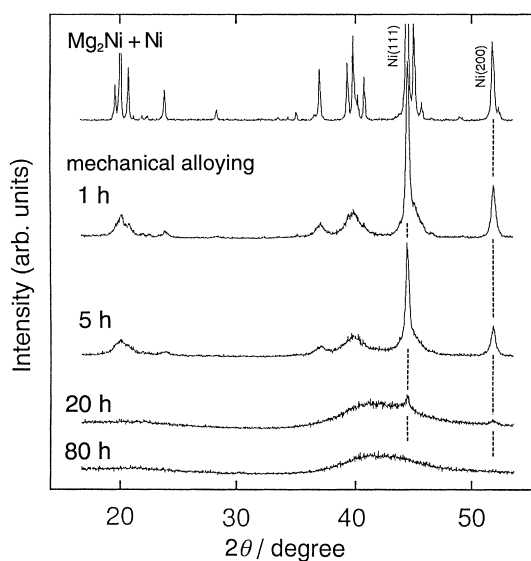


Fig. 1. X-ray diffraction profiles of MgNi during mechanical alloying. The major diffraction peaks, except those of elemental Ni, correspond to Mg $_2$ Ni.

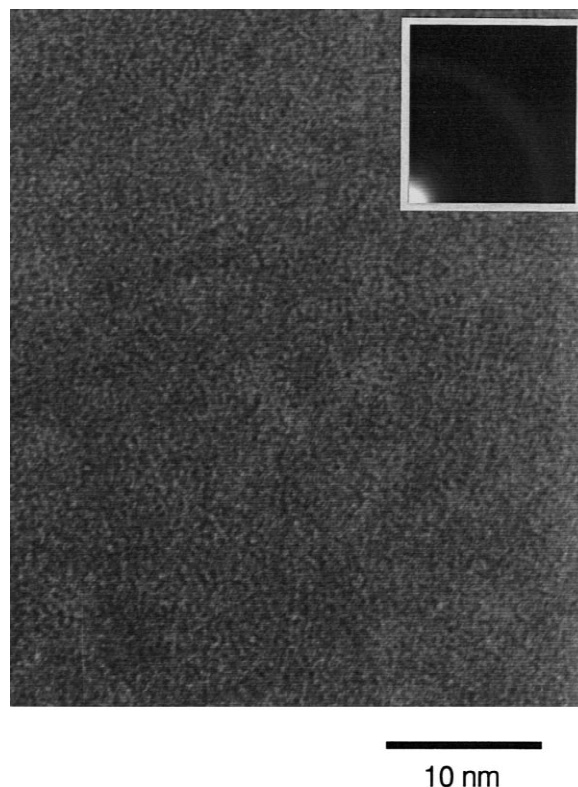


Fig. 2. High resolution TEM image and diffraction pattern of MgNi mechanically alloyed for 80 h.

miscibility-gap (plateau) pressure, even in the amorphous phase. This experimental result directly shows that the site-energy distribution for hydrogen in MgNi is narrow enough for the occurrence of the spinodal decomposition [27]. So far, for conventional amorphous phases, such as ZrNi, no miscibility-gap pressure has been observed due to their wide site-energy distribution [28–31]. Site-energy distributions predominantly come from the variation of neighboring metal atoms around hydrogen atoms. In the

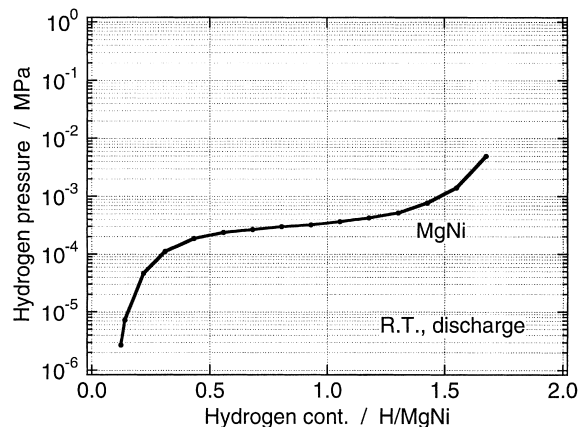


Fig. 3. Electrochemical p - c isotherm of MgNi (in the discharge process at room temperature).

amorphous phase of ZrNi, for example, there are several types of nearest metal coordinations with different site-energies, increasing from 4Zr to 1Zr3Ni or 4Ni.

It should be also noted that the miscibility-gap pressure of MgNi locates around 3×10^{-4} MPa at room temperature. In Mg_2NiH_4 with stable covalent-type bonding composed of Mg^{2+} and $[\text{NiH}_4]_4$ -complex [2–5], the miscibility-gap pressure extrapolated to room temperature is of the order of 10^{-6} MPa [32].

To understand the origin of the hydriding properties described above, X-ray and neutron diffraction profiles was analyzed to obtain accurate information on the metal–deuterium correlations in dilutely and fully deuterided MgNi, that is, $\text{MgNiD}_{0.1}$ and $\text{MgNiD}_{1.6}$, respectively.

First, for $\text{MgNiD}_{1.6}$, the obtained distribution functions $RDF(r)^X$ and $RDF(r)^N$ are shown in the upper part of Fig. 4. The large single peak around $r=0.270$ nm in $RDF(r)^X$ corresponds to the metal–metal (Mg–Mg, Mg–Ni and Ni–Ni) correlations. In order to clarify the Mg–D correlations, the contribution of the metal–metal correlation was eliminated [15], and the result is shown in the lower part of Fig. 4. The coordination numbers n and interatomic distances r of the Mg–D and Ni–D correlations in MgNi were determined by least-squares fitting using Gaussian peak profiles shown in Fig. 4. The results are summarized in Table 1. This table directly shows that deuterium in MgNi occupies the tetrahedral site composed of nearly $2\text{Mg}2\text{Ni}$, and implies that the local atomic structure is also similar to the CsCl-type structure at least in the deuterided (hydrogenated) state at room temperature.

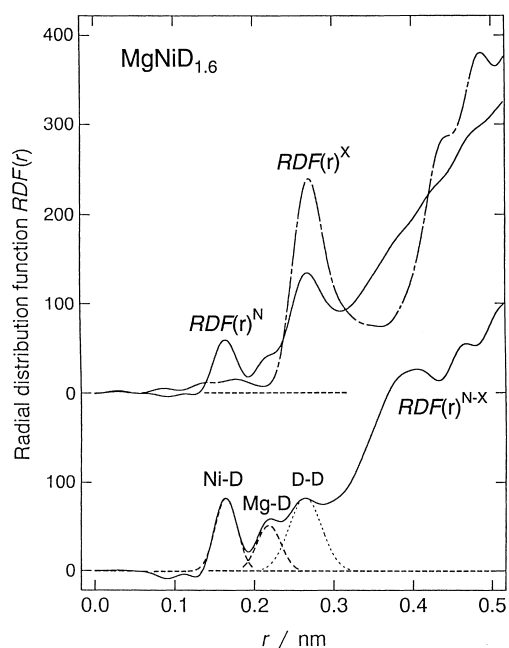


Fig. 4. Upper part: Total radial distribution function for X-ray diffraction $RDF(r)^X$ and that for neutron diffraction $RDF(r)^N$ of $\text{MgNiD}_{1.6}$. Lower part: Subtracted total radial distribution function $RDF(r)^{N-X}$ of $\text{MgNiD}_{1.6}$.

Table 1

The coordination numbers n and interatomic distances r of the Mg–D and Ni–D correlation in $\text{MgNiD}_{1.6}$

| | n | r |
|------|---------------|----------------------|
| Mg–D | 2.3 ± 0.3 | 0.218 ± 0.003 nm |
| Ni–D | 1.7 ± 0.3 | 0.164 ± 0.003 nm |

Next, the distribution function $RDF(r)^N$ obtained for $\text{MgNiD}_{0.1}$ is shown in Fig. 5. The coordination numbers and interatomic distances are shown in Table 2. In spite of the limited accuracy caused by the very-small content of deuterium, it could be confirmed that the Ni–D coordination exists even in this system. The Mg-rich coordination corresponds reasonably to the low-pressure equilibrium of hydrogen in dilutely deuterided (hydrogenated) MgNi, as shown in Fig. 3.

Specific hydrogen configuration in MgNi dissimilar to that in Mg_2Ni [2–5,33] were also detected by the high-resolution proton NMR measurements [34].

The restricted type of nearest metal coordination in MgNi, that is nearly $2\text{Mg}2\text{Ni}$, can explain the narrower site-energy distribution for hydrogen compared to that of the conventional amorphous phase, and the weaker chemical-bonding compared to that of Mg_2NiH_4 . The restricted coordination is the origin of the p – c isotherm shown in Fig. 3.

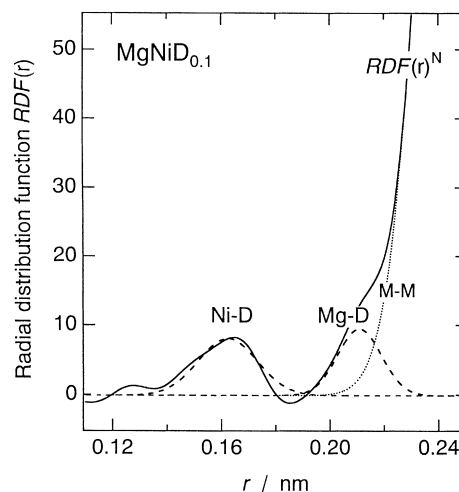


Fig. 5. Total radial distribution function for neutron diffraction $RDF(r)^N$ of $\text{MgNiD}_{0.1}$.

Table 2

The coordination numbers n and interatomic distances r of the Mg–D and Ni–D correlation in $\text{MgNiD}_{0.1}$

| | n | r |
|------|---------------|--------------------|
| Mg–D | 2.6 ± 0.5 | 0.21 ± 0.01 nm |
| Ni–D | 1.7 ± 0.5 | 0.16 ± 0.01 nm |

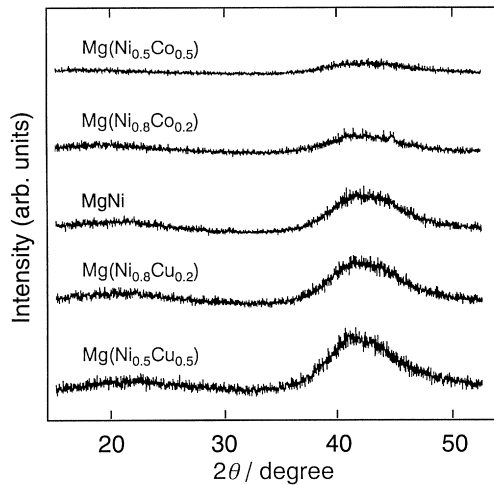


Fig. 6. X-ray diffraction profiles of $\text{Mg}(\text{Ni}_{1-x}\text{T}_x)$ ($\text{T}=\text{Co}$ and Cu) with $x=0, 0.2$ and 0.5 .

3.2. Ni replacement by Co and Cu [16,18]

Fig. 6 shows the X-ray diffraction profiles of $\text{Mg}(\text{Ni}_{1-x}\text{T}_x)$ ($\text{T}=\text{Co}$ and Cu). After the mechanical alloying for 80 h, amorphous phases are formed over the entire composition range. The maximum positions of the halos only in the Cu-substitution shift to lower angles. This result shows that averaged interatomic distances in amorphous phases are expanded by the Cu substitution, reflecting that the atomic size of Cu is 2–3% larger than that of Co or Ni. In the Co substitutions, the intensities are weakened because of the X-ray absorption by Co.

The profiles of differential thermal analysis of $\text{Mg}(\text{Ni}_{1-x}\text{T}_x)$ are shown in Fig. 7. The crystallization of MgNi proceeds in two steps; the first exothermic reaction

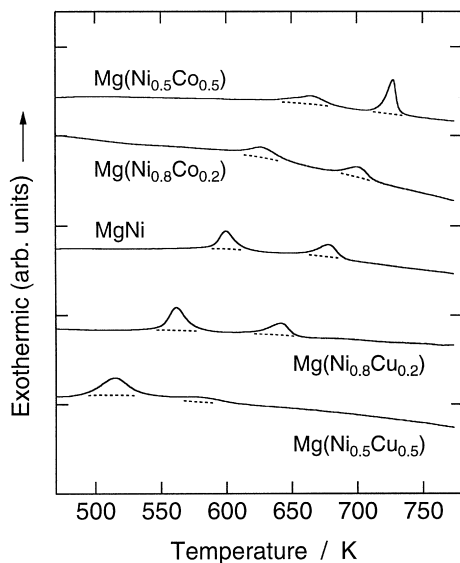


Fig. 7. Profiles of differential thermal analysis of $\text{Mg}(\text{Ni}_{1-x}\text{T}_x)$ ($\text{T}=\text{Co}$ and Cu) with $x=0, 0.2$ and 0.5 . The first exothermic reactions correspond to the partial crystallization into Mg_2Ni , and the second ones into MgNi_2 .

at 596 K corresponds to the partial crystallization into Mg_2Ni , and the second one at 676 K into MgNi_2 [7,11–13]. Fig. 7 shows that the two-step process is substantially valid also for the Co- and Cu-substitutions, and that both crystallization temperatures increase/decrease by the Co-/Cu-substitution, respectively. These phenomena are caused by the increase/decrease of the activation energies for the crystallization [16,35].

In the p - c isotherm of $\text{Mg}(\text{Ni}_{0.5}\text{T}_{0.5})$ shown in Fig. 8, the isotherm becomes steep by the Co- and Cu-substitutions. This result indicates that the distribution of hydrogen-site energies becomes wider, and also that different types of the nearest metal coordinations, like $2\text{Mg}1\text{Ni}1\text{T}$ and $2\text{Mg}2\text{T}$ -sites, are formed in addition to the $2\text{Mg}2\text{Ni}$ -site [18]. Especially, the Cu-substitution results in a wider site-energy distribution for hydrogen and a steeper miscibility-gap pressure compared to that in the Co-substitution. The hydriding properties, which were obtained by the p - c isotherm measurements, can be quantitatively explained by the rule of reversed stability [36–38] of $\text{Mg}(\text{Ni}_{0.5}\text{T}_{0.5})$; the detailed discussion is presented in Ref. [18].

3.3. Mg replacement by Al [15,17]

Fig. 9 shows the X-ray diffraction profiles of $(\text{Mg}_{1-x}\text{Al}_x)\text{Ni}$. The amorphous phase is formed in the range $x=0$ – 0.2 , while the crystalline phase of a CsCl-type structure is formed for $x=0.3$ – 0.5 . All the diffraction peaks are rather broad, coming from nanometer-scale crystallites with a high lattice defect concentration. The interatomic distances estimated from maximum positions of the halo profiles and from the (110) diffraction peaks in Fig. 9 continuously decrease with increasing Al concentration, reflecting that the atomic size of Al is 10% smaller than that of Mg.

The profiles of differential thermal analysis of $(\text{Mg}_{1-x}\text{Al}_x)\text{Ni}$ are shown in Fig. 10. For $x=0.1$, the two-step process mentioned in 3.2 still exists, although

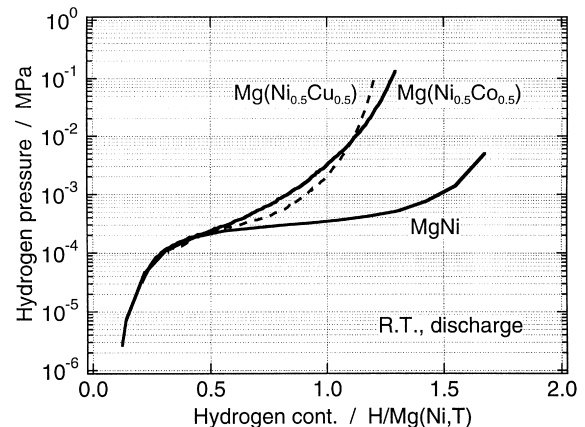


Fig. 8. Electrochemical p - c isotherms of $\text{Mg}(\text{Ni}_{1-x}\text{T}_x)$ ($\text{T}=\text{Co}$ and Cu) with $x=0$ and 0.5 (in the discharge processes at room temperature).

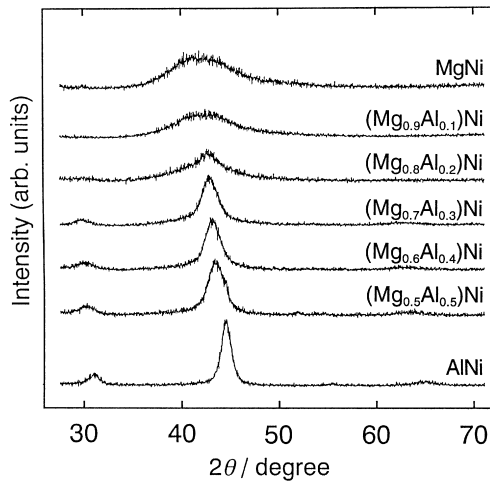


Fig. 9. X-ray diffraction profiles of $(\text{Mg}_{1-x}\text{Al}_x)\text{Ni}$ with $x=0, 0.1, 0.2, 0.3, 0.4$ and 0.5 . The profile of the intermetallic compound AlNi mechanically milled for 80 h is also shown as a reference.

both exothermic reactions shift to nearly 30 K higher temperatures caused by the increment of activation energies for the crystallization. The peak area of each exothermic reaction for $x=0.1$, especially that of the second one, decreases as compared with that of $x=0$. This result qualitatively suggests that the amorphous phase with $x=0.1$ is more stable than that with $x=0$. In contrast, almost no exothermic reaction corresponding to the crystallization is observed for $x=0.3$ in the temperature ranges mentioned above. This result indicates that the crystalline phase with a CsCl-type structure is thermally stabilized at this composition.

In the p - c isotherm of $(\text{Mg}_{1-x}\text{Al}_x)\text{Ni}$ shown in Fig. 11, the miscibility-gap pressure increases from $x=0$ to $x=0.1$, and reaches almost 1×10^{-3} MPa. The pressure increase is attributed to the decrease of interatomic distances, and also

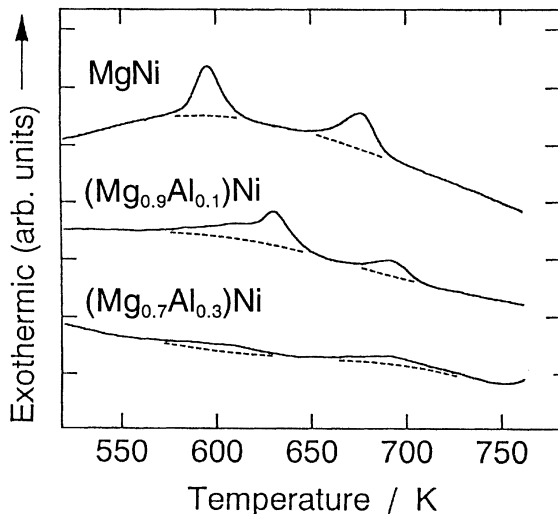


Fig. 10. Profiles of differential thermal analysis of $(\text{Mg}_{1-x}\text{Al}_x)\text{Ni}$ with $x=0, 0.1$ and 0.3 .

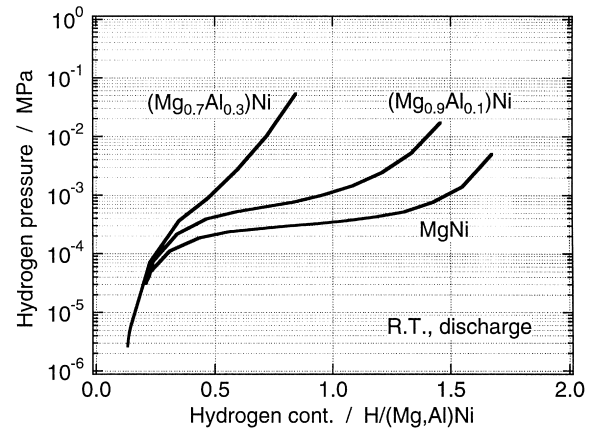


Fig. 11. Electrochemical p - c isotherms of $(\text{Mg}_{1-x}\text{Al}_x)\text{Ni}$ with $x=0, 0.1$ and 0.3 (in the discharge processes at room temperature).

to the lower affinity of elemental Al with hydrogen [39]. The slope of the isotherm becomes steep for $x=0.3$, mainly because of the nanometer-scale crystallites with a high lattice defect concentration [40–44]. Heat treatments for both the grain-growth and strain-release of crystallites are necessary for further improvements of the hydriding properties.

4. Conclusions

The electrochemical p - c isotherm measurement on MgNi revealed that there is an obvious miscibility-gap pressure higher than 10^{-4} MPa at room temperature, even in the amorphous phase. The total radial distribution functions show that deuterium in MgNi occupies the interstitial tetrahedral site composed of nearly $2\text{Mg}_2\text{Ni}$.

The amorphous phases are also formed over the entire composition range of $\text{Mg}(\text{Ni}_{1-x}\text{T}_x)$ ($\text{T}=\text{Co}$ and Cu) with $x=0$ – 0.5 . The crystallization temperatures increase/decrease by Co/Cu -substitution, respectively. The p - c isotherm measurements indicate that the site-energy distribution for hydrogen become wider, and that different types of the nearest metal coordinations are newly formed.

In $(\text{Mg}_{1-x}\text{Al}_x)\text{Ni}$, the amorphous phase is also formed with $x=0$ – 0.2 , while the crystalline phase of a CsCl-type cubic structure is formed with $x=0.3$ – 0.5 . The miscibility-gap pressure increases for $x=0.1$ with the amorphous phase, attributing to the decrease of interatomic distances, and also to the lower affinity of elemental Al with hydrogen. The slope of the isotherm becomes steep for $x=0.3$ by the formation of the nanometer-scale crystallites.

Acknowledgements

The authors would like to acknowledge to Professor Y. Kitano and Dr. K. Yamamoto for valuable TEM observation, and also to Dr. G. Majer for the critical reading of the

manuscript. A part of this work was financially supported from the New Energy and Industrial Technology Development Organization (NEDO). One of the authors (SO) sincerely acknowledges the financial support provided from the Electric Technology Research Foundation of Chugoku (travel support) and also from the Alexander von Humboldt foundation.

References

- [1] A. Percheron-Guégan, J.-M. Welter, in: L. Schlapbach (Ed.), Topics in Applied Physics, Hydrogen in Intermetallic Compounds I, Vol. 63, Springer-Verlag, Berlin/Heidelberg, 1988, p. 11.
- [2] K. Yvon, J. Less-Common Met. 103 (1984) 53.
- [3] M. Gupta, L. Schlapbach, in: L. Schlapbach (Ed.), Topics in Applied Physics, Hydrogen in Intermetallic Compounds I, Vol. 63, Springer-Verlag, Berlin/Heidelberg, 1988, p. 139.
- [4] D. Noréus, K. Jansson, M. Nygre, Z. Phys. Chem. 146 (1985) 191.
- [5] Y. Takahashi, H. Yukawa, M. Morinaga, J. Alloys Comp. 242 (1996) 98.
- [6] J.J. Reilly, R.H. Wiswall Jr., Inorg. Chem. 7 (1968) 2254, Recently, we have experimentally confirmed that the mechanical grinding promotes a hydriding reaction of the MgNi₂.
- [7] Q.M. Yang, Y.Q. Lei, C.P. Chen, J. Wu, Q.D. Wang, G.L. Lu, L.S. Chen, Z. Phys. Chem. 183 (1994) 141.
- [8] D.L. Sun, Y.Q. Lei, W.H. Liu, J.J. Jiang, J. Wu, Q.D. Wang, J. Alloys Comp. 231 (1995) 621.
- [9] C. Iwakura, S. Nohara, H. Inoue, Y. Fukumoto, Chem. Commun. 15 (1996) 1831.
- [10] W.H. Liu, H.Q. Wu, Y.Q. Lei, Q.D. Wang, J. Alloys Comp. 252 (1997) 234.
- [11] S. Orimo, K. Ikeda, H. Fujii, Y. Fujikawa, Y. Kitano, K. Yamamoto, Acta Mater. 45 (1997) 2271.
- [12] S. Orimo, H. Fujii, K. Ikeda, Y. Fujikawa, Y. Kitano, Proc. International Symposium on Metal–Hydrogen Systems – Fundamentals and Applications, Les Diablerets, Switzerland, August 25–30, 1996, J. Alloys Comp. 253–254 (1997) 94.
- [13] S. Orimo, H. Fujii, Intermetallics 6 (1998) 185.
- [14] K. Funaki, S. Orimo, H. Fujii, J. Alloys Comp. 270 (1998) 160.
- [15] S. Orimo, K. Ikeda, H. Fujii, S. Saruki, T. Fukunaga, A. Züttel, L. Schlapbach, Acta Mater. 46 (1998) 4519.
- [16] S. Orimo, K. Ikeda, H. Fujii, K. Yamamoto, J. Alloys Comp. 260 (1997) 143.
- [17] S. Orimo, K. Ikeda, H. Fujii, J. Alloys Comp. 266 (1998) L1.
- [18] K. Ikeda, S. Orimo, A. Züttel, L. Schlapbach, H. Fujii, J. Alloys Comp. 280 (1998) 279.
- [19] K. Suzuki, M. Misawa, K. Kai, N. Watanabe, Nucl. Instr. Meth. 147 (1977) 519.
- [20] T. Fukunaga, PhD Thesis, Tohoku University, 1978.
- [21] T. Fukunaga, Physica B 213–214 (1995) 518.
- [22] S. Orimo, H. Fujii, K. Ikeda, Acta Mater. 45 (1997) 331.
- [23] A. Züttel, F. Meli, L. Schlapbach, J. Alloys Comp. 203 (1994) 235.
- [24] A. Züttel, F. Meli, L. Schlapbach, J. Alloys Comp. 231 (1995) 645.
- [25] A. Züttel, D. Chartouni, K. Gross, M. Bächler, L. Schlapbach, Proc. International Symposium on Metal–Hydrogen Systems – Fundamentals and Applications, Les Diablerets, Switzerland, August 25–30, 1996, J. Alloys Comp. 253–254 (1997) 587.
- [26] K. Yamamoto, Y. Fujikawa, K. Ikeda, S. Orimo, H. Fujii, Y. Kitano, J. Electron Microsc. 47 (1998) 467.
- [27] Y. Fukai (Ed.), The Metal–Hydrogen System – Basic Bulk Properties, Springer-Verlag, New York, 1992, p. 57.
- [28] F.H.M. Spit, J.W. Drijver, S. Radelaar, Scr. Metall. 14 (1980) 1071.
- [29] R. Kirchheim, F. Sommer, G. Schluckebier, Acta Metall. Mater. 30 (1982) 1059.
- [30] K. Aoki, M. Kamachi, T. Masumoto, J. Non-Cryst. Solid 61–62 (1984) 679.
- [31] J.H. Harris, W.A. Curtin, M.A. Tenhover, Phys. Rev. B 16 (1987) 5784.
- [32] K. Nomura, E. Akiba, S. Ono, Int. J. Hydrogen Energy 6 (1981) 295.
- [33] K. Yvon, P. Fischer, in: L. Schlapbach (Ed.), Topics in Applied Physics, Hydrogen in Intermetallic Compounds I, Vol. 63, Springer-Verlag, Berlin/Heidelberg, 1988, p. 87.
- [34] S. Hayashi, S. Orimo, H. Fujii, J. Alloys Comp. 261 (1997) 145.
- [35] K.H.J. Buschow, N.M. Beekmans, Solid State Commun. 35 (1980) 233.
- [36] A.R. Miedema, J. Less-Common Met. 32 (1973) 117.
- [37] H.H. van Mal, K.H.J. Buschow, A.R. Miedema, J. Less-Common Met. 35 (1974) 65.
- [38] Y. Tsushio, E. Akiba, J. Alloys Comp. 269 (1998) 219.
- [39] R. Griessen, T. Riesterer, in: L. Schlapbach (Ed.), Topics in Applied Physics, Hydrogen in Intermetallic Compounds I, Vol. 63, Springer-Verlag, Berlin, Heidelberg, 1992, p. 266.
- [40] T. Mütschele, R. Kirchheim, Scr. Metall. 21 (1987) 135.
- [41] T. Mütschele, R. Kirchheim, Scr. Metall. 21 (1987) 1101.
- [42] R. Kirchheim, T. Mütschele, W. Kieninger, H. Gleiter, R. Birringer, T.D. Koblé, Mat. Sci. Eng. 99 (1988) 457.
- [43] R.J. Wolf, M.W. Lee, J.R. Ray, Phys. Rev. Lett. 73 (1994) 557.
- [44] L. Zaluski, P. Tessier, D.H. Ryan, C.B. Doner, A. Zaluska, J.O. Ström-Olsen, M.L. Trudeau, R. Schulz, J. Mater. Res. 8 (1993) 3059.